evaluate some relevant observables such as the time distribution for fusion and the kinetic energy distribution of non-fusion events which can hardly be accessed in a fully quantal framework. Here, we restrict the study to collisions between ^{64}Ni nuclei. Fig. 5 shows five illus-

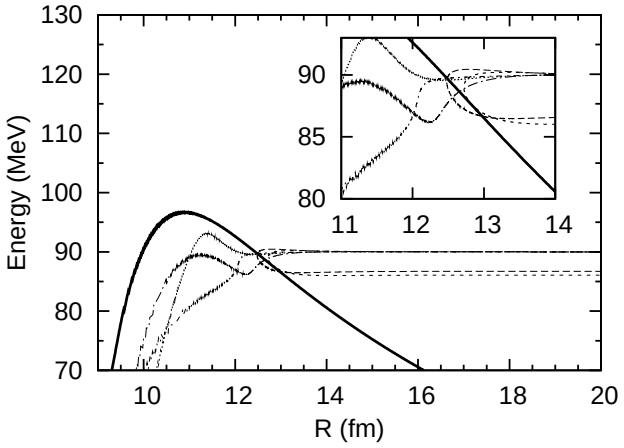

FIG. 5: The center of mass energies for five sample events, with incident energy of 90 MeV, are plotted versus the relative distance of two ^{64}Ni nuclei. The center of mass energy is the sum of the first four terms in Eq. (1), hence it is the energy of the relative motion. The angular momentum is set to zero. The s-wave potential barrier is shown for the bare case where there is no coupling to the surface modes (thick line).

trative events as a function of relative distance of ^{64}Ni ions for head-on collisions at bombarding energy of 90 MeV. In this figure, the thick line indicates the bare potential. Even though the bombarding energy is below the bare barrier, as a result of barrier fluctuations, three of the five events end up fusing, while two events after inelastic collision re-separate. During inelastic collisions, part of the incident energy is dissipated by excitations of the surface vibrations. Using the ensemble of events generated for description of the collision process, we can calculate the final kinetic energy distributions of the non-fusion events. The upper panel (a) of Fig. 6 shows final kinetic energy distributions of non-fusion events at different incident energies in head-on collisions of ^{64}Ni + ^{64}Ni systems, while the lower panel (b) presents the final kinetic energy distributions for different relative angular momenta at an incident energy of 96 MeV. As it is expected, the mean final energy increases with the incident energy as well as with the angular momentum. The variances of the distributions increase as incident energy increases and angular momentum decreases. Indeed, in this case, the rates of non-fusion events decrease eventually increasing the uncertainty of the final energy. Fig. 7 illustrates the average value of the final energy of the relative motion of non-fusion events. It is observed that, at very low incident bombarding energies, almost no energy is transferred to surface excitations. As the energy increases, the amount of dissipated energy into the sur-

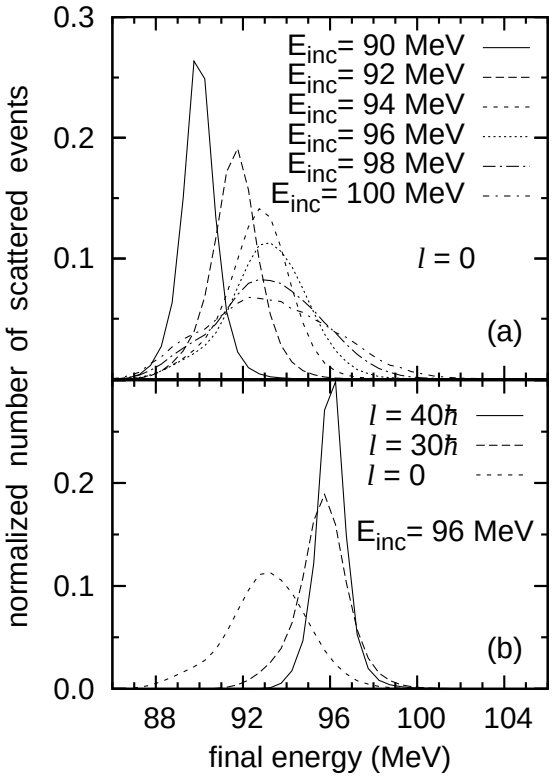

FIG. 6: The distribution of the final energy of non-fusing events in collisions of ^{64}Ni nuclei is plotted for different incident center of mass energies (a) and different angular momenta (b). For each plot the distribution function is normalized with the total number of scattered (no-fusion) events.

face modes increases. After the energy exceeds the fusion barrier height at $V_B = 96.5$ MeV, the mean final energy is almost constant indicating that the total excitation energy $E^\star$ is almost linearly increasing with the incident energy. In the simulations of the trajectories, we take the initial relative distance as $R = 20$ fm. We call the event as a fusion event, if the trajectory evolves all the way until the separation distance reaches to $R = 5$ fm. For fusion events, we define the time it takes to travel from $R = 20$ fm to $R = 5$ fm as the fusion time. The upper panel (a) of Fig. 8 indicates the distribution of fusion times at different incident energies in central collisions of nickel ions, while the lower panel (b) shows the fusion time distributions for three different orbital angular momenta at incident energy of 96 MeV. Again, as we expect, the mean fusion time increases with increasing angular momentum and decreasing incident energy.

V. CONCLUSION

Employing a stochastic semi-classical model for low-energy heavy-ion collisions, which was proposed origi-